

Atomic-Resolution Electron Energy Loss Spectroscopy Imaging in Aberration Corrected Scanning Transmission Electron Microscopy

L. J. Allen,¹ S. D. Findlay,¹ A. R. Lupini,² M. P. Oxley,¹ and S. J. Pennycook²

¹*School of Physics, University of Melbourne, Victoria 3010, Australia*

²*Oak Ridge National Laboratory, Solid State Division, P.O. Box 2008, Oak Ridge, Tennessee 37831-6030, USA*

(Received 12 March 2003; published 5 September 2003)

The “delocalization” of inelastic scattering is an important issue for the ultimate spatial resolution of innershell spectroscopy in the electron microscope. It is demonstrated in a nonlocal model for electron energy loss spectroscopy (EELS) that delocalization of scanning transmission electron microscopy (STEM) images for single, isolated atoms is primarily determined by the width of the probe, even for light atoms. We present experimental data and theoretical simulations for Ti *L*-shell EELS in a [100] SrTiO₃ crystal showing that, in this case, delocalization is not significantly increased by dynamical propagation. Issues relating to the use of aberration correctors in the STEM geometry are discussed.

DOI: 10.1103/PhysRevLett.91.105503

PACS numbers: 61.14.-x, 61.85.+p, 68.37.Lp

Innershell electron energy loss spectroscopy (EELS) has become a powerful tool for determining structure-property relationships at interfaces and grain boundaries, probing local stoichiometry, impurity segregation, and electronic structure. When acquired simultaneously with an atomic-resolution *Z*-contrast image in scanning transmission electron microscopy (STEM), very high spatial resolution has been demonstrated [1–4]; impurity concentrations and local *d*-band occupancies can be measured from individual atomic columns at grain boundaries and interfaces [5]. However, the ability to place a probe over a single column does not guarantee that the EELS signal is generated at that column. Here we examine the delocalization of the STEM image which, for a given probe, is determined not only by the ionization process itself but also by dynamical diffraction. Delocalization is, loosely speaking, the quantum equivalent of the classical impact parameter [6,7]. We take the practical measure of this to be the width of the signal in a STEM image from an atom or atomic column and it is in this sense that we use the term. How the delocalization compares to atomic or column spacings is central to reliably inferring structure using innershell spectroscopy for atomically resolved analyses.

In the *Z*-contrast image, formed from high-angle thermally scattered electrons, sub-angstrom information transfer has already been demonstrated [8], and promises to become routine with the regular inclusion of spherical aberration correctors for the probe-forming lens [9,10]. The *Z*-contrast image is dominated by Rutherford scattering from the screened nuclear potential, and is highly localized. It has been well-established that *Z*-contrast images give a good indication of structure [11]; the peaks which sometimes arise in open channels [12] can often be attributed to the probe tails and may, in a first approximation, be removed using deconvolution to separate out the effects of the probe [13]. The fidelity of such *Z*-contrast images means that comparison between simul-

taneously collected *Z*-contrast and EELS data provides a method of judging experimentally how well the EELS signal represents the structure.

It has recently been demonstrated that, for the case of *Z* contrast, the dynamical nature of probe propagation may lead to an appreciable contribution to the signal from columns adjacent to that on which the probe is situated, the so-called “cross-talk” phenomenon [14,15]. Using simulations in which the ionization interaction is treated in a full nonlocal manner, similar cases have been found for EELS [15]. This suggests that caution should be taken in interpreting experimental EELS images. We present calculations of STEM images from a single, isolated atom, a scenario which eliminates any effect of probe propagation. The calculations show that delocalization of the EELS image in such a case is limited by the size of the probe rather than the nature of the ionization interaction. We further show that, in the case of a zone-axis SrTiO₃ crystal, through examination of the Ti *L*-shell EELS image, the resolution remains dominated by the probe and column-by-column spectroscopy is achieved.

Our simulations of inelastic STEM images use the mixed dynamic form factor (MDFF) approach [14–16]. For EELS, the MDFFs may be formed in a fully nonlocal calculation, or by using the local approximation [17–20]. Here we use the nonlocal model to describe the inelastic scattering event [21–23]. Cross-section expressions (i.e., incoherent images) may then be calculated using either a Bloch wave or a multislice method. Selection between the two methods is based upon convenience, since the results of the two methods have been shown to be in excellent agreement [16]. It should be noted that this formulation includes a diffuse background term which gives the contribution to the images from dechanneled electrons.

Quantum mechanical calculations of delocalization have been inconsistent, some predicting significant delocalization [24,25] and others much less [26,27]. In the local approximation, the effective scattering potential

may be plotted in real space. Delocalization may then be assessed in terms of the width of the peaks. However, it has been shown that EELS simulations often need to be done using the fully nonlocal model [17–20] and such a potential is difficult to visualize spatially. Thus, we shall discuss delocalization not of the interaction potential but rather of the resultant STEM image, which is what is measured experimentally.

Figure 1 shows the three probes to be considered. Probe 1 contains no aberrations, and uses a reciprocal space aperture cutoff of 1.0 \AA^{-1} . Probe 2 is aberration balanced, being characterized by $\{C_s = -0.05 \text{ mm}, C_5 = 63 \text{ mm}, \Delta f = 62 \text{ \AA}, \text{cutoff} = 0.539 \text{ \AA}^{-1}\}$ (where C_s denotes third order spherical aberration, C_5 denotes fifth order spherical aberration, and Δf denotes defocus with overfocus taken to be positive). This set characterizes the experiment to be discussed. Probe 3 uses $C_s = 0.5 \text{ mm}$ and Scherzer conditions, chosen as it is broader again. Figures 2(a) and 2(b) show, for the different probes, the Ti L -shell and O K -shell EELS STEM line scans of isolated Ti and O atoms, respectively. The Ti L edge occurs at an energy loss of 507 eV, the O K edge at 564 eV. The simulations use a 20 mrad collection angle and a 40 eV energy window above the ionization thresholds. It is seen that the full width at half maximum of the image gets progressively broader as we move from the first and finest probe to the third and broadest. Thus, the delocalization of the STEM image is affected by the properties of the probe, even in the case of a light atom such as oxygen. We note that for the finest probe the image contains some structure. The “volcano-like” appearance of single atom

images under certain conditions has been previously explained [24].

It should be stressed that this result holds for a single atom. In a crystal, the dynamical nature of propagation may serve to alter any probe in such a way as to change the delocalization of the images. To explore this possibility, the crystalline case will now be examined using SrTiO_3 as a case study.

Experimental line scans of SrTiO_3 were taken using VG Microscopes’s HB501UX microscope at ORNL, equipped with a Nion aberration corrector [28]. The attempt to annul aberrations is accomplished by balancing the lens parameters, as described above for probe 2. The zone axis considered is [100]. The accelerating voltage is 100 keV. The EELS scan is based on Ti L -shell ionization, with a detector half angle of 20 mrad, and an energy window of 40 eV above the ionization threshold. Line scans are taken along the [011] direction in which Sr columns alternate with combined Ti and O columns. The Z-contrast scan used an annular detector range of 56–202 mrad.

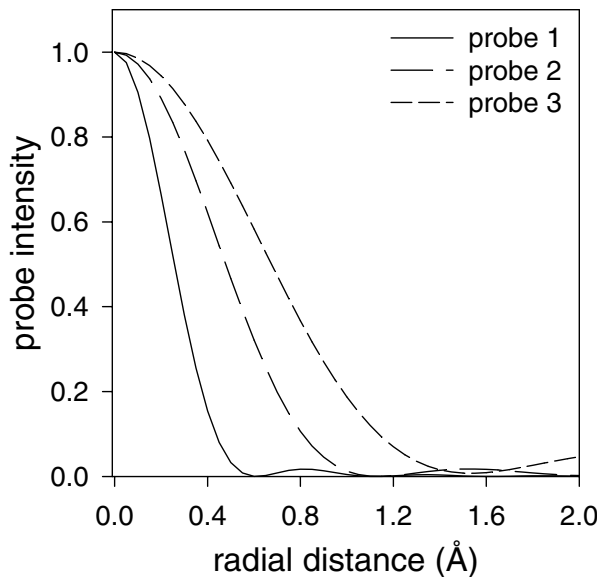


FIG. 1. Intensity profiles of the three probes under consideration. Probe 1 is an aberration-free probe with 1.0 \AA^{-1} aperture cutoff, probe 2 is an aberration balanced probe with 0.539 \AA^{-1} aperture cutoff, and probe 3 has $C_s = 0.5 \text{ mm}$ and Scherzer conditions.

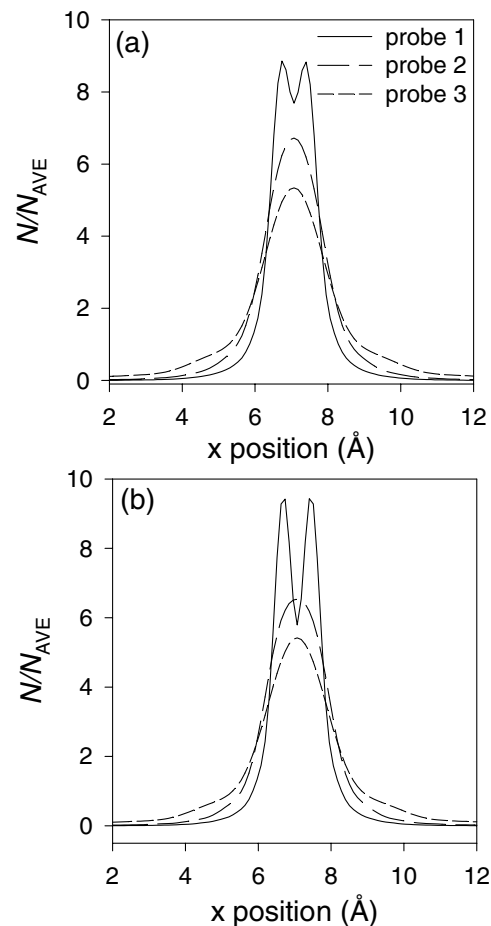


FIG. 2. (a) Ti L -shell EELS STEM image of a single, isolated titanium atom; (b) O K -shell EELS STEM image of a single, isolated oxygen atom. Plots are given for the probes shown in Fig. 1.

Figure 3 shows the experimental line scans for Z contrast and Ti L -shell EELS in SrTiO_3 , scaled by their average value for convenience of display. The ADF signal clearly alternates between strong and weak peaks at a spacing consistent with the known structure of SrTiO_3 (cubic, at room temperature, with side length 3.9 \AA). The bright peaks are taken to be the Sr columns, the weaker peaks then are the Ti/O columns. Simulations bear this out; in no parameter set investigated was the ratio between the columns reversed. Taking the peaks of the Z -contrast signal as indicative of these columns, it may be seen that the EELS signal does indeed give peaks corresponding to the Ti/O column positions. The thickness of the crystalline region is gauged to be approximately 200 \AA . As ion milling was used in specimen preparation, it is expected that there will be amorphous surface layers present in addition to this. The fluctuation in the signals, and the distinct variation between the two adjacent cells, may be attributed to physical instability in the microscope and the presence of amorphous surface layers.

The dynamical nature of probe propagation makes it unclear as to whether the behavior observed in the single atom case will carry over to crystalline experiments. The drive for aberration correction is based on the assumption that it will, that finer probes will lead to higher resolution images. To investigate this assumption, simulations of the Ti L -shell EELS STEM image for SrTiO_3 are presented for the three probes used previously. (Approximate Debye-Waller factors for SrTiO_3 were obtained from the literature [29] for use in the calculations. Simulations showed little dependence in the contrast of the images for moderate variation of these factors.) Figure 4 shows the results, and also plots the experimental data for comparison purposes.

It is seen that the behavior described in the single atom case, specifically that finer probes lead to finer features in

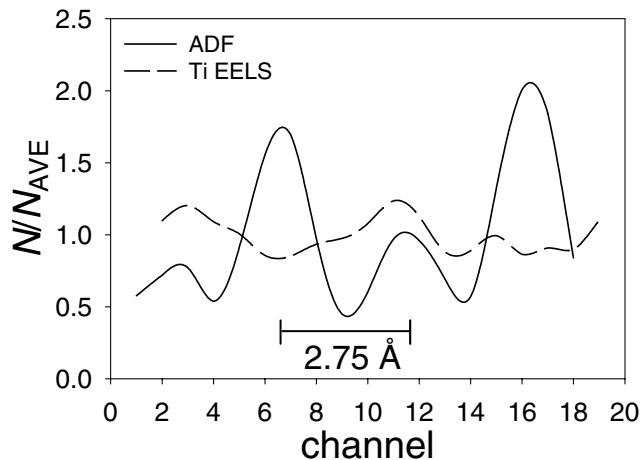


FIG. 3. Experimental data plots showing the ADF (Z contrast) and Ti L -shell EELS results. Experimental parameters as given in the text.

the STEM image, has carried over to the crystalline case under consideration. Decreasing the width of the probe leads to a decrease in the width of the column peaks, and an enhancement of the contrast.

Such a result is not unexpected. It has been shown previously [15,30] that the majority of the dynamical signal comes from the initial portion of the crystal, where probe spreading and absorption have not yet begun to dominate the behavior of the wave function. That said, it is clear from Fig. 4 that the finer probes pick up a significant contribution to the Ti EELS signal on the Sr columns. This is the result of the thermal background. The Sr column, with a high atomic number, causes significant “absorption” due to thermal diffuse scattering. The degree of absorption is enhanced with the finer probe because of the greater electron density on the atomic column [31]. The resultant background of dechanneled electrons is less localized to the site of the probe than the dynamical wave function and so may cause ionization on the adjacent Ti columns. It should be stressed that this is a dynamical result. It will not be removable by deconvolution of the probe as has been used previously in the ADF regime [13]. Such behavior as this will complicate the direct interpretation of EELS STEM images at such high resolutions, and motivates the need for detailed simulation as part of the interpretation process.

While the plot for probe 3 in Fig. 4 most closely follows the data, it is probe 2 which characterizes the experiment. There are many reasons for the quantitative discrepancies between simulation and experiment. The simulations presented here do not account for amorphous

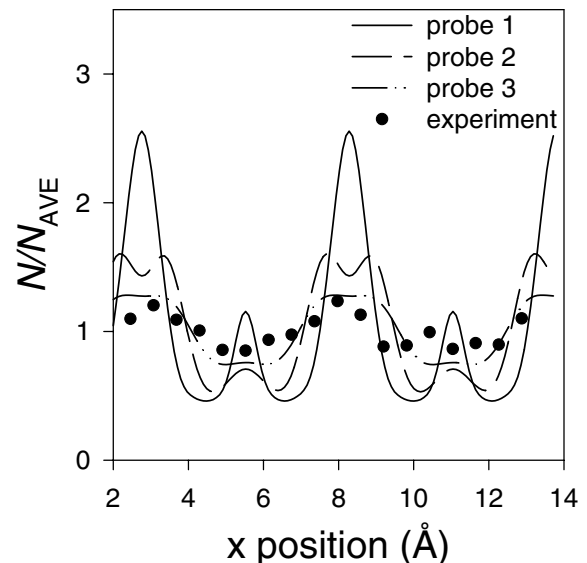


FIG. 4. Simulated data plots showing the Ti L -shell EELS results in the full nonlocal calculation for a perfect crystal of thickness 200 \AA using the three probes of Fig. 1. The experimental data is also plotted. The parameters used in the experiment and the simulation are described in the text.

surface layers, chromatic aberration, or spatial instability in the probe. Taking some combination of these factors into account can significantly improve the quantitative agreement. However, without a more detailed characterization of the specimen and the probe, it was deemed inappropriate to treat these quantities as open parameters in an attempt to investigate quantitative agreement between theory and experiment, since there would be no valid consistency check on the results. As such, we cannot say from this data whether the mismatch problem between simulations and experiment which is known in the TEM geometry [32] manifests in STEM. The focus of this discourse is rather on the delocalization of the signal and the implications for the use of aberration correctors in the STEM geometry.

We have demonstrated, by means of simulating STEM images of single atoms, that it is the width of the probe, rather than the nature of the ionization interaction, which limits the width of single atom features in EELS, even for the lighter atoms. This motivates the drive for aberration correction, implying that finer probes will indeed yield finer features. In the presence of dynamical diffraction in a zone-axis crystal, we have presented experimental data, in conjunction with theoretical simulations, which support the fact that the EELS signal is confined to the expected column. These results support the notion that finer features are obtained with finer probes. However, some of the features, such as the significant contribution from columns which do not contain the atomic species characterized by the detected energy loss, become more difficult to interpret by visual means alone. Therefore the ability to perform detailed EELS simulations may become a necessary adjunct to experimentally obtained data. The combination of simulation and experiment provides a powerful tool for structural and chemical analysis to high resolution.

This research was sponsored by the Laboratory Directed Research and Development Program of Oak Ridge National Laboratory managed by UT-Battelle, LLC for the U.S. Department of Energy under Contract No. DE-AC05-00OR22725, by appointment to the ORNL Postdoctoral Research Program administered jointly by ORNL and ORISE and by the Australian Research Council.

-
- [1] N. D. Browning, M. F. Chisholm, and S. J. Pennycook, *Nature (London)* **366**, 143 (1993).
 - [2] D. A. Muller, Y. Tzou, R. Raj, and J. Silcox, *Nature (London)* **366**, 725 (1993).
 - [3] P. E. Batson, *Nature (London)* **366**, 727 (1993).
 - [4] D. A. Muller, S. Subramanian, P. E. Batson, J. Silcox, and S. L. Sass, *Acta Mater.* **44**, 1637 (1996).

- [5] G. Duscher, N. D. Browning, and S. J. Pennycook, *Phys. Status Solidi A* **166**, 327 (1998).
- [6] A. Howie, *J. Microsc.* **117**, 11 (1979).
- [7] J. C. H. Spence and J. Lynch, *Ultramicroscopy* **9**, 267 (1982).
- [8] P. D. Nellist and S. J. Pennycook, *Phys. Rev. Lett.* **81**, 4156 (1998).
- [9] O. L. Krivanek, N. Dellby, and A. R. Lupini, *Ultramicroscopy* **78**, 1 (1999).
- [10] S. J. Pennycook, B. Rafferty, and P. D. Nellist, *Microsc. Microanal.* **6**, 343 (2000).
- [11] P. D. Nellist and S. J. Pennycook, *Ultramicroscopy* **78**, 111 (1999).
- [12] K. Watanabe, T. Yamazaki, Y. Kikuchi, Y. Kotaka, M. Kawasaki, I. Hashimoto, and M. Shiojiri, *Phys. Rev. B* **63**, 085316 (2001).
- [13] A. J. McGibbon, S. J. Pennycook, and D. E. Jesson, *J. Microsc.* **195**, 44 (1999).
- [14] L. J. Allen, S. D. Findlay, M. P. Oxley, and C. J. Rossouw, *Ultramicroscopy* **96**, 47 (2003).
- [15] C. J. Rossouw, L. J. Allen, S. D. Findlay, and M. P. Oxley, *Ultramicroscopy* **96**, 299 (2003).
- [16] S. D. Findlay, L. J. Allen, M. P. Oxley, and C. J. Rossouw, *Ultramicroscopy* **96**, 65 (2003).
- [17] M. P. Oxley and L. J. Allen, *Acta Crystallogr. Sect. A* **56**, 470 (2000).
- [18] L. J. Allen and T. W. Josefsson, *Phys. Rev. B* **52**, 3184 (1995).
- [19] M. P. Oxley and L. J. Allen, *Phys. Rev. B* **57**, 3273 (1998).
- [20] M. P. Oxley and L. J. Allen, *Acta Crystallogr. Sect. A* **57**, 713 (2001).
- [21] B. Rafferty and S. Pennycook, *Ultramicroscopy* **78**, 141 (1999).
- [22] V. W. Maslen and C. J. Rossouw, *Philos. Mag. A* **49**, 735 (1984).
- [23] C. J. Rossouw and V. W. Maslen, *Philos. Mag. A* **49**, 743 (1984).
- [24] H. Kohl and H. Rose, *Adv. Imaging Electron Phys.* **65**, 173 (1985).
- [25] D. A. Muller and J. Silcox, *Ultramicroscopy* **59**, 195 (1995).
- [26] O. F. Holbrook and D. M. Bird, in *Proceedings of the Conference on Electron Microscopy and Analysis*, edited by D. Cherns [*Inst. Phys. Conf. Ser.* **147**, 175 (1995)].
- [27] B. Rafferty and S. J. Pennycook, *Ultramicroscopy* **78**, 141 (1999).
- [28] N. Dellby, O. L. Krivanek, P. D. Nellist, P. E. Batson, and A. R. Lupini, *J. Electron Microsc.* **50**, 177 (2001).
- [29] L. M. Peng, *Acta Crystallogr. Sect. A* **53**, 663 (1997).
- [30] S. Hillyard, R. F. Loane, and J. Silcox, *Ultramicroscopy* **49**, 14 (1993).
- [31] C. Dwyer and J. Etheridge, *Ultramicroscopy* **96**, 343 (2003).
- [32] M. J. Hytch and W. M. Stobbs, *Ultramicroscopy* **53**, 191 (1994).